GPS Solutions (2022) 26:149
https://doi.org/10.1007/s10291-022-01340-1

ORIGINAL ARTICLE

Copula, a new approach for optimum design of Voxel-based GNSS tropospheric tomography based on the atmospheric dynamics

Roya Mousavian[1,2] · Masoud Mashhadi Hossainali[1] · Christof Lorenz[2] · Harald Kunstmann[2,3]

Received: 23 December 2021 / Accepted: 22 September 2022

Abstract

Global Navigation Satellite System (GNSS) signals scan the earth's atmosphere with a high spatiotemporal resolution. They have promoted the application of the GNSS networks as an imaging system for the tomographic reconstruction of wet refractivity (N_w).To come up with a unique solution of this inverse problem and to preserve the atmospheric dynamics intact by solution, the resolution of reconstructed images of wet refractivityis usually increased. We propose a Copula-based approach as a geometry-free technique to develop a tomography network over southwest Germany and a part of France. Here, we apply the estimated N_w time series from Weather Research and Forecasting model from April to October 2016 and evaluate the pixel-wise dependence structure and dissimilarity measures of the N_w time series at seven pressure levels from 949.2 to 263.8 hPa. At each level, the most appropriate dissimilarity measure to give an optimal resolution is identified based on the percentage of pair pixels with asymmetric Copulas. Then, the optimum resolution is identified by evaluating the distance-based variations of dissimilarity values. The investigations propose a non-uniform tomography network for this region. Furthermore, we assess the geometry of the problem by investigating the resolution matrix of the tomography model in all hourly time epochs of Day of Year (DoY) 279. According to the results, using uniform voxel size for tomography reconstruction in the area leads to missing information in the lower parts of the troposphere. Moreover, we show that combining our method and resolution matrix provides a mathematical tool for deciding on the required compromise between the geometry and dynamics in Global Positioning System (GPS) tomography.

Keywords Atmospheric modeling · Copula · Correlation · Dependence · Dissimilarity measures · GNSS tomography

Introduction

Global Navigation Satellite System (GNSS) meteorology is a powerful tool for estimating the integrated water vapor (IWV) with an accuracy better than 1–3 mm (Bevis et al. 1992; Lee et al. 2013). The high-resolution estimates of IWVs can be assimilated into numerical weather prediction (NWP) models to improve their quality (de Haan et al. 2009). GNSS tomography is a technique to provide water vapor with a high resolution using GNSS signals (Bevis et al. 1992; Rohm 2012). Due to the spatiotemporal variations of water vapor, voxel-based tomography is usually the preferred approach (Vaquero-Martinez and Anton 2021) where the study region is spatially discretized into several 3D-elements (voxels) with invariable water vapor during a given period of time. The voxel collection is known as the tomography network or model. Slant tropospheric delays (STD) on GNSS signals crossing these voxels are then inverted to water vapor field. Therefore, the quality of the tomographic reconstruction is related to the voxel dimension (Bi et al. 2006; Notarpietro et al. 2011).

The distribution of the GNSS receivers and satellites has an essential impact on voxel sizes or the spatial resolution of a tomography model. Increasing the model resolution, i.e., decreasing the size of voxels, increases the number of unknowns. In other words, while smaller voxel sizes increase the number of empty elements and affect

✉ Roya Mousavian
r_mousavian@yahoo.com; roya_mousavian@mail.kntu.ac.ir

[1] Faculty of Geodesy and Geomatics Engineering, K. N. Toosi University of Technology, No. 1346, ValiAsr Street, Mirdamad cross, Tehran, Iran

[2] Institute of Meteorology and Climate Research (IMK-IFU), Karlsruhe Institute of Technology, Kreuzeckbahnstr. 19, 82467 Garmisch-Partenkirchen, Germany

[3] Institute of Geography, University of Augsburg, Alter Postweg 118, 86159 Augsburg, Germany

Published online: 03 October 2022

the uniqueness and precision of the solution, larger voxel sizes reduce the accuracy of the solution (Notarpietro et al. 2011). Most of the previous studies empirically define the size of voxels. Optimal horizontal voxel size is sometime determined by investigating the resolution matrix (a measure for analyzing the uniqueness of the solution) of the corresponding model for different voxel sizes (Adavi and Mashhadi-Hossainali 2014). Chen and Liu (2014) proposed to relocate the tomographic area based on tomography condition to improve the utilization of signal rays. Yao and Zhao (2017) evaluated the non-uniform symmetrical division of voxels horizontally based on the number of passing signals from different parts of the tomography network (i.e., center or edge). Sadeghi et al. (2022) proposed a method based on the principal component analysis to optimize the horizontal resolution of GPS tomography model.

In this study, we propose a geometry-free Copula-based method to determine the voxel sizes in a tomography model. Copula functions fully describe the dependence structure of variables (any statistical relationship such as linear or nonlinear relations between the variables). The method firstly introduced by Sklar (1959) and, because of its flexibility, has been widely used in different disciplines such as economics and finance (Ang and Chen 2002;), hydrology (Bardossy and Li 2008), meteorology (Vogl et al. 2012) and remote sensing (Lorenz et al. 2018). However, using Copulas in geodesy is generally new and limited to three individual research areas, polar motion prediction (Modiri et al. 2018, 2020) and investigating the dependence structure of zenith tropospheric delays (Mousavian et al. 2021).

We use Copulas for modeling the dependence structure of the wet refractivities (N_w) estimated from the Weather Research and Forecasting (WRF) model from April to October 2016 (Skamarock et al. 2008). We further design a tomography network by analyzing Copula-based dissimilarity measures and the dependence structure of wet refractivities across our study region. Then, we consider the consistency of our proposed method with the constraints that the imaging system geometry imposes on this problem using the resolution matrix. Since the technique is based on a long-term analysis of the N_w parameters, the proposed model is independent of time for the time length of the applied WRF data. This is a significant step toward improving the accuracy of GNSS tomography in real-time applications.

The main objectives of this study are: (a) to design a tomography network using Copula theory, (b) to compare this method with the implied results from the resolution matrix of the model and (c) to propose an optimum size for the voxels which is consistent with satellite–receiver imaging geometry and atmospheric dynamics. A summary and outlook follow the sections.

Methodology

The voxel-based GPS tomography is based on the assumption that the water vapor in each voxel is constant during the applied temporal resolution. That is, reconstructed tomographic images not only report on N_w values but also provide information on the dynamics of this parameter. We incorporate the dynamics of the problem by deciding on the spatial resolution of our model by analyzing the Copula-based dependence structure and dissimilarity measures of wet refractivities in a test area. Furthermore, the uniqueness of the GPS tomography results for a Copula-based designed network is investigated using a resolution matrix. Therefore, in addition to the Copula-based method, GPS tomography and resolution matrix are briefly given.

Introduction to Copula

Copulas are mathematical functions that join multivariate distribution functions to their univariate marginals and fully describe the dependence structure of variables as follows (Sklar 1959; Nelsen 2006):

$$F(x_1, x_2, ..., x_n) = C(F_1(x_1), F_2(x_2), ..., F_n(x_n)) \tag{1}$$

where F is an n-dimensional cumulative distribution function (CDF) of random variables $x_i \in \mathbb{R},\ i = 1, 2, ..., n$, $F_1, F_2, ..., F_n$ are univariate marginal distributions of x_i and C is an n-dimensional Copula.

Therefore, for every $n \geq 2$, an n-dimensional Copula, $C : [0, 1]^n \rightarrow [0, 1]$ is an n-dimensional CDF whose univariate marginals are uniformly distributed on [0, 1]. Then, the multivariate Copula density function is given by:

$$c(F_1(x_1), F_2(x_2), ..., F_n(x_n)) = \frac{\partial^n C(F_1(x_1), F_2(x_2), ..., F_n(x_n))}{\partial F_1(x_1) ... \partial F_n(x_n)} \tag{2}$$

For simplicity, this study is restricted to the application of bivariate Copulas. Generally, there are two types of parametric Copulas: implicit and explicit. The implicit ones are derived from the known multivariate distribution functions and do not have a closed mathematical form. Gaussian Copula which is a symmetric Copula derived from the standardized multivariate Gaussian distribution $\Phi_R(\mathbf{0}, \mathbf{R})$ with zero mean and correlation matrix $\mathbf{R}$ is the most familiar one from this category and is defined by (Mikosch 2006),

$$C_R^{Ga}(\mathbf{u}) = \Phi_R(\Phi^{-1}(u_1), \Phi^{-1}(u_2)) \tag{3}$$

where $u_i,\ i = 1, 2$ are univariate marginal distributions of variables and $\Phi^{-1}(\cdot)$ is the inverse of the standard univariate normal CDF. The density of this bivariate Copula can be estimated by (Arbenz 2013):

$$c(\mathbf{u}) = \frac{1}{\sqrt{\det(\mathbf{R})}} \exp(-1/2(\mathbf{X}^T(\mathbf{R}^{-1} - \mathbf{I})\mathbf{X})) \quad (4)$$

here $\mathbf{I}$ is the identity matrix and $X = (\Phi^{-1}(u_1), \Phi^{-1}(u_2))^T$

In contrast, explicit Copulas can be expressed in closed mathematical form. The most important and widely used type of these Copulas is the family of Archimedean Copulas and for $u_i \in [0,1], \quad i = 1,2$ as the marginals of random variables $x_i, \ i = 1,2$ the family is given by (Embrechts et al. 2001; Nelsen 2006)

$$C_\phi(u_1, u_2) = \phi^{-1}\{\phi(u_1) + \phi(u_2)\}, \ \mathbf{u} \in [0,1]^2 \quad (5)$$

where $\phi[0,1] \rightarrow [0,\infty)$ is the generator function of the Copula C_ϕ. Archimedean Copulas are described by the generator functions, which contain all the information on the dependence structure of random variables.

Table 1 indicates the closed forms of four widely used Archimedean Copulas which are investigated in this study, together with their generator functions and the range of their parameters. They are the family of Clayton, Gumbel, Ali–Mikhail–Haq (AMH) and Frank Copulas. Figure 1 shows the dependence structure of these Copulas and the Gaussian one. Since the range of Copula parameters for all families is not the same, different Copula parameters are used. In these figures u_1 and u_2 are uniform variables on [0,1] and $c\ (u_1, u_2)$ is their Copula densities. According to Fig. 1, all these Copulas except the Frank and the Gaussian have asymmetric dependence structures. The Clayton and AMH Copulas are more correlated in the lower tail much more strongly for the Clayton, and the Gumbel Copula shows significant upper tail dependence. Therefore, these Archimedean Copulas, together with the Gaussian one, are sufficient for modeling every kind of dependence in our data.

Copula-based dissimilarity measures

Dissimilarity measures are numerical values that indicate how different two objects or data sets are and quantify the independency (or dependency) of variables. Many dissimilarity measures with their pros and cons are developed over the years (Goshtasby 2012). We apply the Copula-based dissimilarity measures, which are based on empirical Copula distribution and density (Samaniego et al. 2010). Therefore, the dissimilarity measures are given after expressing the required statistical concepts and empirical quantities for their estimation.

Estimation of marginal distributions

The first step in all Copula-based investigations is estimating the univariate marginal distributions and transforming the input data to the unit interval [0, 1] or rank space. If there is no a priori information about the random variable X and its distribution, but a sufficient number of samples T is available, the empirical distribution with the following formulas is a good approximation of the true underlying distribution (Charpentier et al. 2007):

$$u_i = \hat{F}_i(x) = \frac{1}{T+1} \sum_{t=1}^{T} I(X_t^i \leq x), \ i = 1,2 \quad (6)$$

where $I(\cdot)$ denotes the indicator function and is defined as

$$I_A(x) := \begin{cases} 1 & x \in A \\ 0 & x \notin A \end{cases} \quad (7)$$

here A is any non-empty subset of set X.

Empirical Copula distribution

The empirical Copula was introduced as an empirical dependence function that converges to the underlying Copula (Deheuvels 1979; Nelsen 2006). This empirical Copula CDF is estimated by

$$\hat{C}(u_{1j}, u_{2j}) = \frac{1}{T} \sum_{t=1}^{T} I(\hat{F}_1(x_{1t}) \leq u_{1j}, \hat{F}_2(x_{2t}) \leq u_{2j}), \quad j = 1,2,...,T \quad (8)$$

where $\hat{F}_i(x_i), \quad i = 1,2$, and T and $I(\cdot)$ are the univariate marginal distributions of the random variables $x_i, i = 1,2$, sample size and the indicator function, respectively.

Table 1 Most common Archimedean Copulas, their generator functions and the range of the Copula parameter θ

Family	$\phi(t)$	θ	$C_\theta(u_1, u_2)$
Clayton	$\frac{t^{-\theta}-1}{\theta}$	$(0,\infty)$	$(u_1^{-\theta} + u_2^{-\theta} - 1)^{-\frac{1}{\theta}}$
Gumbel	$(-\log(t))^\theta$	$[1,\infty)$	$\exp\left\{-[(-\log(u_1))^\theta + (-\log(u_2))^\theta]^{\frac{1}{\theta}}\right\}$
Frank	$\log\left(\frac{e^{\theta t}-1}{e^\theta-1}\right)$	$\mathbb{R}\backslash\{0\}$	$-\frac{1}{\theta}\log\left\{1 + \frac{(e^{-\theta u_1}-1)(e^{-\theta u_2}-1)}{e^{-\theta}-1}\right\}$
Ali–Mikhail–Haq (AMH)	$\frac{\ln(1-\theta(1-t))}{t}$	$[-1,1]$	$\frac{u_1 u_2}{1-\theta(1-u_1)(1-u_2)}$

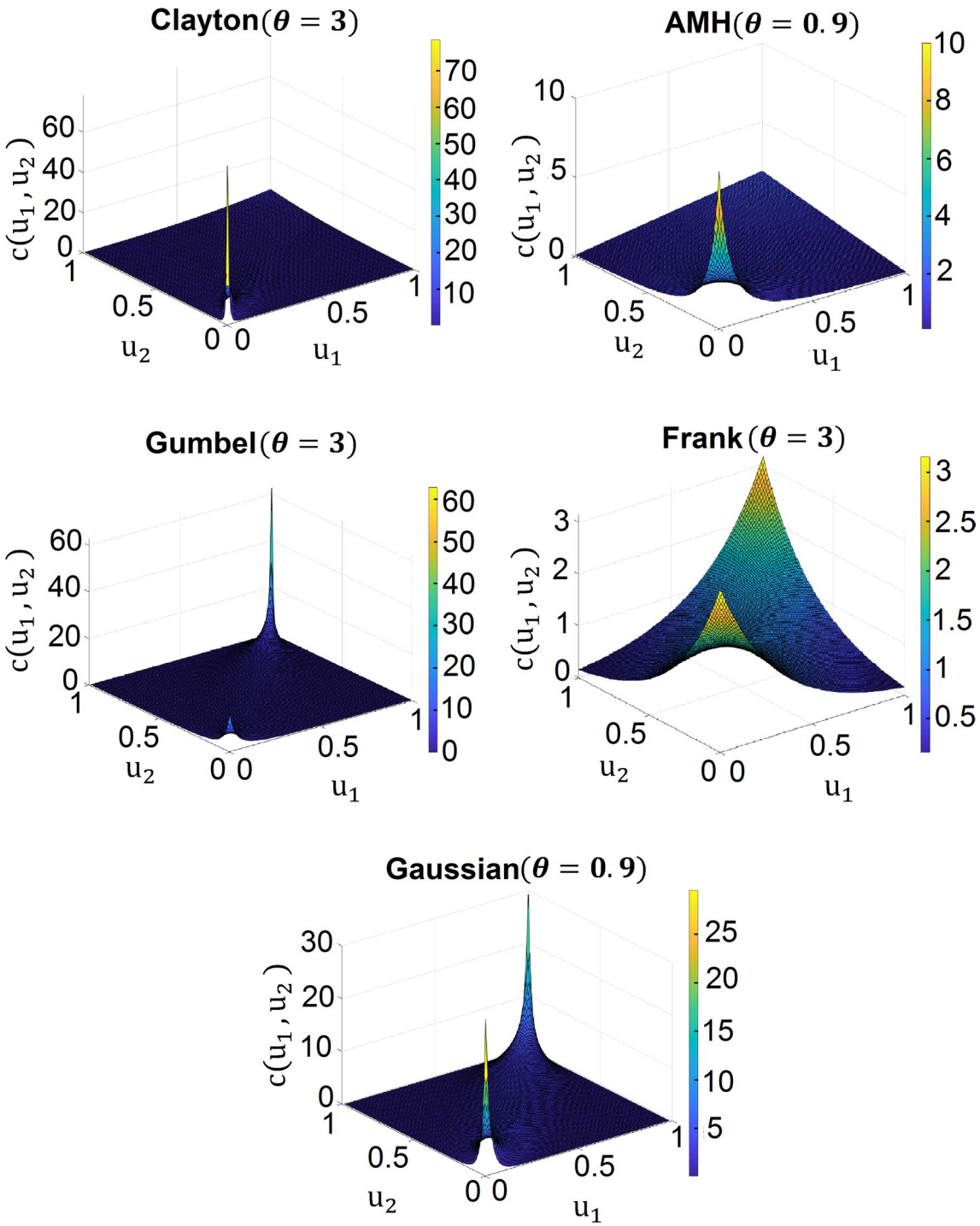

Fig. 1 Copula densities of the applied families for bivariate samples (μ_1, μ_2) with two different Copula parameters (θ) based on their meaningful ranges

Empirical Copula density

Similar to the empirical Copula CDF, the empirical Copula PDF can be estimated from the data through nonparametric methods (Charpentier et al. 2007). Thus, the empirical Copula PDF is calculated by discretizing the interval between 0 and 1 to a regular $k \times k$ grid based on the sample size as follows (Bardossy 2006; Nelsen 2006)

$$\hat{c}\left(\frac{2r-1}{2k}, \frac{2s-1}{2k}\right) = \frac{k^2}{T} q_{rs} \tag{9}$$

where T and q_{rs} are sample size and the empirical frequency corresponding to the grid coordinates (r, s) with $\{r, s = 1, 2, \ldots, k\}$, respectively. For a given pair, q_{rs} is

$$q_{rs} = \left| \left\{ \frac{r-1}{k} < u_1 < \frac{r}{k} and \frac{s-1}{k} < u_2 < \frac{s}{k} \right\} \right| \tag{10}$$

here $u_i, i = 1, 2$ are the univariate marginal distributions in the rank space and $|\cdot|$ is the cardinality (the number of elements of a set). To ensure that the dependence between random variables is accurately represented, the sample size should be large enough, i.e., $T > 5k^2$ (Samaniego et al. 2010).

Dissimilarity measures

Three different Copula-based dissimilarity measures, i.e., λ^1, λ^2 and λ^3 have been developed (Samaniego et al. 2010). λ^1 for every two variables u_i and u_j in a set with n pairs of variables is defined by tail dependence which describes how one marginal distribution exceeds a certain threshold given that the other margin has already exceeded that threshold:

$$\lambda_{ij}^1 = (P - L_{ij}) + \frac{|U_{ij} - L_{ij}|}{U_{ij} + L_{ij}} \tag{11}$$

where P is a given probability threshold, (e.g., 0.2) which separates tails from the rest of the distribution. U_{ij} and L_{ij} are the upper and the lower tail probabilities of the empirical Copula density $\hat{c}$, respectively:

$$L_{\mathrm{ij}} = \int_0^P \int_0^P \hat{c}(u_i, u_j) \mathrm{d}u_i \mathrm{d}u_j \tag{12}$$

$$U_{\mathrm{ij}} = \int_{1-P}^1 \int_{1-P}^1 \hat{c}(u_i, u_j) \mathrm{d}u_i \mathrm{d}u_j \tag{13}$$

As the empirical Copula densities are given on a regular grid, the integrals can be transformed into sums.

This dissimilarity measure consists of two terms: The first term estimates how far the empirical Copula density is from a perfect lower corner dependence, and the second one describes the level of asymmetry of the upper and lower tails about the axis $u_j = 1 - u_i$.

The second measure λ^2 does not require any pre-defined parameters and is given as

$$\lambda_{\mathrm{ij}}^2 = (1 - r_{\mathrm{ij}}) + \xi \left| A_{\mathrm{ij}} \right| \tag{14}$$

where ξ is a scaling factor which is selected so that $\sup(1 - r_{ij}) \approx \sup \left| A_{ij} \right|$. r_{ij} and A_{ij} are Spearman's rank correlation, which is computed from the empirical Copula (see (8)), and the degree of asymmetry of the empirical Copula density, respectively. They are calculated by

$$r_{\mathrm{ij}} = 12 \int_0^1 \int_0^1 (\hat{C}(u_i, u_j) - u_i u_j) \mathrm{d}u_i \mathrm{d}u_j \tag{15}$$

$$A_{\mathrm{ij}} = \int_0^1 \int_0^1 \left[\left(u_i - \frac{1}{2} \right)^2 \left(u_j - \frac{1}{2} \right) + \left(u_i - \frac{1}{2} \right) \left(u_j - \frac{1}{2} \right)^2 \right] \hat{c}(u_i, u_j) \mathrm{d}u_i \mathrm{d}u_j \tag{16}$$

Therefore, the first and second terms of λ^2 describe the statistical dependence between variables and the dissimilarity due to the asymmetry of their empirical Copulas, respectively.

The third dissimilarity measure consists of the asymmetry of Copula density (i.e., A_{ij}, see (9)) and the Kolmogrov–Smirnov statistic $\left(M_{ij}\right)$ as follows:

$$\lambda_{\mathrm{ij}}^3 = M_{\mathrm{ij}} + \xi \left| A_{\mathrm{ij}} \right| \tag{17}$$

where

$$M_{ij} = \sup \left| H\left(\Delta x_1(t)\right) - H(\Delta x_2(t)) \right| \tag{18}$$

here t is time in the time series and H is the distribution function of the lag one differences of each variable time series, that is, $\Delta x(t) = x(t) - x(t-1)$.

Therefore, the second and third dissimilarity measures are free of any pre-defined parameters and are more general. Furthermore, according to Samaniego et al. (2010), λ^1 has only moderate sensitivity to extreme values and the asymmetry of the Copula density. Hence, λ^2 and λ^3 should be preferred for variables that are correlated in the tails of their distributions.

Copula-based dependence structure modeling

The Copula-based dependence structure modeling contains several steps, i.e., (1) the transformation of data to the rank space, (2) the estimation of theoretical Copulas, (3) estimating empirical Copula CFD and PDFs, and (4) the identification of best-fitted Copula. Except for steps 1 and 3, which are explained in the previous subsections, other steps are described in the following (refer to Mousavian et al. (2021) for details).

Theoretical Copula and parameter estimation

For Copula parameter estimation, in the case of variables with unknown marginal distribution, the semi-parametric methods like canonical maximum likelihood (CML) (Cherubini et al. 2004) are preferred to fully parametric methods, e.g., maximum likelihood (ML) (Joe 1997). Hence, we apply

the CML estimation in this study. The method consists of using empirical marginal distributions for transforming sample data $\{x_{1t}, x_{2t}\}_{t=1}^{T}$ to the rank space $\{u_{1t}, u_{2t}\}_{t=1}^{T}$ and computing the corresponding Copula parameter using a maximum likelihood estimate:

$$\hat{\theta} = \text{Arg Max}_{\theta} \sum_{t=1}^{T} \ln c\left(\hat{F}_1(x_{1t}), \hat{F}_2(x_{2t}); \theta\right) \tag{19}$$

where $c(u_{1t}, u_{2t}; \theta)$ is the theoretical copula density with its parameters θ (see (2) and (4) and Table 1) and *ArgMax* refers to the θ values at which the summation of the logarithm of the Copula density are maximized.

Copula selection

There is a wide range of methods for identifying the most appropriate Copula. Except for the Bayesian method (Huard et al. 2006), the selection approaches usually require estimating the Copula parameters in advance. The goodness-of-fit (GOF) criteria are the most common approaches for Copula selection. According to Fang et al. (2014) and Guloksuz (2016), for bivariate Archimedean Copulas Akaike information criterion (AIC) and Bayesian information criterion (BIC) outperform other GOF criteria. Therefore, we apply these approaches in this study.

The AIC and BIC for bivariate Copulas are defined as:

$$AIC = -2 \sum_{t=1}^{T} \ln[c(u_{1t}, u_{2t}); \theta] + 2k \tag{20}$$

$$BIC = -2 \sum_{t=1}^{T} \ln[c(u_{1t}, u_{2t}); \theta] + \ln(Tk) \tag{21}$$

where $c(u_{1t}, u_{2t})$ is the Copula density, T is the sample size and k is the number of parameters in the desired Copula. The most suitable Copula is identified by comparing AIC and BIC values for different Copulas. Lower values of AIC and BIC indicate a better fit to the data.

GNSS tomography

The GNSS tropospheric tomography is a technique to model the spatiotemporal variations of the water vapor using the GNSS signals. Through this method, the study area is divided into several cubic elements known as voxels and the wet refractivity (N_w) is reconstructed in the voxels. The input data of the tomography model are signal slant wet delays (SWDs) which are estimated by the GNSS data processing. The SWD is linked to the N_w by the following equation (Rohm and Bosy 2009):

$$\mathbf{SWD} = \mathbf{AN}_{\mathrm{w}} \tag{22}$$

where $\mathbf{A} = [a_{ij}]$ is an $n \times m$ matrix in which a_{ij} is the length of ith signal traveling through the jth voxel. Here, n and m are the number of signals and the number of unknowns, respectively. The wet refractivity is assumed to change only from one voxel to another, so the number of unknown parameters is the number of voxels in the model.

GNSS signals do not pass through some voxels. Therefore, GNSS tomography is a mixed determined problem without a unique solution. Among the developed methods for computing a unique solution, the application of certain constraints to the system of observation equations is a common one. This research addresses a new method for the determination of the optimum voxel sizes in GNSS tomography. Reducing the size of voxels increases the number of non-trivial elements of **A**. A resolution matrix is normally used to come up with a compromise between voxel sizes and the rank deficiency of the coefficient matrix in (22).

Estimation of resolution matrix

The design matrix of a mathematical model includes all information on the geometry of an inverse problem. In tomography, poor imaging geometry results in the rank deficiency of this matrix and, therefore, destroys the uniqueness of the solution. Assuming a linear inverse problem, the forward and inverse models are given, respectively, by (23) and (24):

$$\mathbf{d} = \mathbf{Gm} \tag{23}$$

$$\underline{\mathbf{m}} = \mathbf{G}^{-g}\mathbf{d} \tag{24}$$

where $\mathbf{G}^{-g}$ is the generalized inverse of rectangular matrix **G**. Replacing the observation vector **d** in (24) by (23), yield (Menke 1989),

$$\underline{\mathbf{m}} = \mathbf{G}^{-g}\mathbf{Gm} \tag{25}$$

where $\mathbf{R}_{m\times m} = \mathbf{G}^{-g}\mathbf{G}$ is known as the model resolution matrix, as a unique characteristic of the design matrix (Aster et al. 2018). Therefore, it can be used in the design phase of an inverse problem. This matrix can be estimated using singular value decomposition (SVD). The singular value decomposition of an $n \times m$ matrix **G** is a factorization of the form $\mathbf{G} = \mathbf{USV}^T$, where **U**, **S** and **V** are an $n \times n$ unitary matrix, an $n \times m$ rectangular diagonal matrix and an $m \times m$ unitary matrix, respectively. Then, $\mathbf{G}^{-g} = \mathbf{VS}^{-1}\mathbf{U}^T$ and the resolution matrix is defined by,

$$\mathbf{R} = \mathbf{V}_p \mathbf{V}_p^T \tag{26}$$

Here $\mathbf{S}$ is the matrix of singular values of $\mathbf{G}$ and p is the number of nonzero singular values. Moreover, the columns of matrices $\mathbf{U}$ and $\mathbf{V}$ are the right and left singular vectors of $\mathbf{G}$, respectively. If the null space of the matrix $\mathbf{G}$ is empty, $\mathbf{R}$ will be an identity matrix. However, if $rank(\mathbf{G}) = p < n$, the resolution matrix of model space is an asymmetric matrix which indicates how far the reconstructed model is from the true model. In other words, if the diagonal elements of the resolution matrix are zero or close to zero, the corresponding parameter will not be well reconstructed (Aster et al. 2018).

Data and study area

Developing a tomography network/model is the first step in GNSS tropospheric tomography. The goal is the determination of the voxel sizes and reconstructing temporal resolution of the model. The basic assumption is that the wet refractivity is homogeneous in every model element. Since relative configuration of the GNSS satellites and tracking points, topography and weather conditions change from one area or time to another, the spatial and temporal resolutions of a model do not remain the same. Wrong choice of these resolutions results in inaccurate reconstruction of the parameters. Moreover, an increasing number of elements lead to instability and loss of accuracy of the solution. Therefore, applying an appropriate method for determining an optimum time and spatial resolution for a tomography model is mandatory. In this study, we concentrate on spatial resolution and propose a geometry-free Copula-based method for this purpose. Its consistency to the resolution matrix in one specific day will be checked as well.

The required data are meteorological parameters that are estimated by a precise numerical weather prediction (NWP) model as well as the coordinate of GPS stations and satellites. Our study area is selected by considering the distribution of permanent GPS stations and radiosondes which are applied to investigate the accuracy of the tomography results. Therefore, parts of southwest Germany and France, including the mountainous and flat areas, have been selected as study regions.

Figure 2 illustrates the topography of our study area together with the distribution of GPS and radiosonde stations. The right-hand side plot shows the location and topography of the study area (red box) relative to the surrounding regions and the left-hand side plot focuses on the study area. In this figure, GNSS and radiosonde stations are denoted by black and red triangles, respectively.

We use the estimated wet refractivities (N_w) from the simulated meteorological parameters in high spatiotemporal resolution from the weather research and forecasting (WRF) model (Fersch et al. 2020), using the following formula,

$$N_w = k_1 \frac{e}{T} + k_3 \frac{e}{T^2} \tag{27}$$

where e and T are water vapor pressure (in hPa) and absolute temperature (in Kelvin), respectively. Also, $k_1 = 77.60K$ hPa^{-1} and $k_3 = 3.739 \times 10^5 K^2$hPa^{-1} are physical constants that are empirically determined (Bevis et al. 1994).

The WRF model was run for Central Europe from April to October 2016. The model was driven by 6-h European Centre for Medium-Range Weather Forecasts (ECMWF) Reanalysis (ERA) Interim (Dee et al. 2011) data, with a spatial resolution of 37 pressure levels from 1000 to 1 hPa. The spatial resolution of WRF was set to 3×3 km, resulting in 315 grid cells in west–east and 280 grid cells in the south–north direction. Fifty vertical layers from 1000 to 10 hPa were further used to get a high-resolution representation of the vertical structure of the atmosphere. In this study, we investigate the troposphere from the earth surface to the 22nd layer, i.e., from the mean pressure of 949.5–263.5 hPa with an approximate geopotential height of 10 km, which is considered as the top of the troposphere in the midlatitude regions.

We use the permanent GNSS stations of the regional network of Germany located in the study area in DoY 279 of the year 2016 for estimating the model space resolution matrix. Due to the high level of humidity, this day is chosen. The network includes approximately 300 stations across Germany (Gendt et al. 2004). Most stations belong to the network Satellite Positioning Service of the German Land Surveying Agencies (SAPOS), and some of them are from the German Federal Agency for Cartography and Geodesy (BKG). We further use the precise satellite ephemerides of the International GNSS Service (IGS).

Copula-based optimum design of tomography model

To design our tomography model, we evaluate the dependence structure of N_w time series across the study area. Due to the lack of passing signals from most voxels, using WRF resolution (3 km) as the horizontal voxel size does not make sense. Therefore, we used the estimated N_w time series (27) in 12 km resolution in our Copula-based analyses. Dissimilarity measures have been computed between the N_w time series of each pixel and other pixels in our study region, for seven pressure layers starting from the earth surface to the top of the troposphere. The applied pressure levels are the earth surface and layers 1, 5, 7, 10, 15 and 22 with the mean pressures of 949.2, 945.9, 896.4, 849.8, 754.9, 519.4 and 263.8 hPa, respectively. For

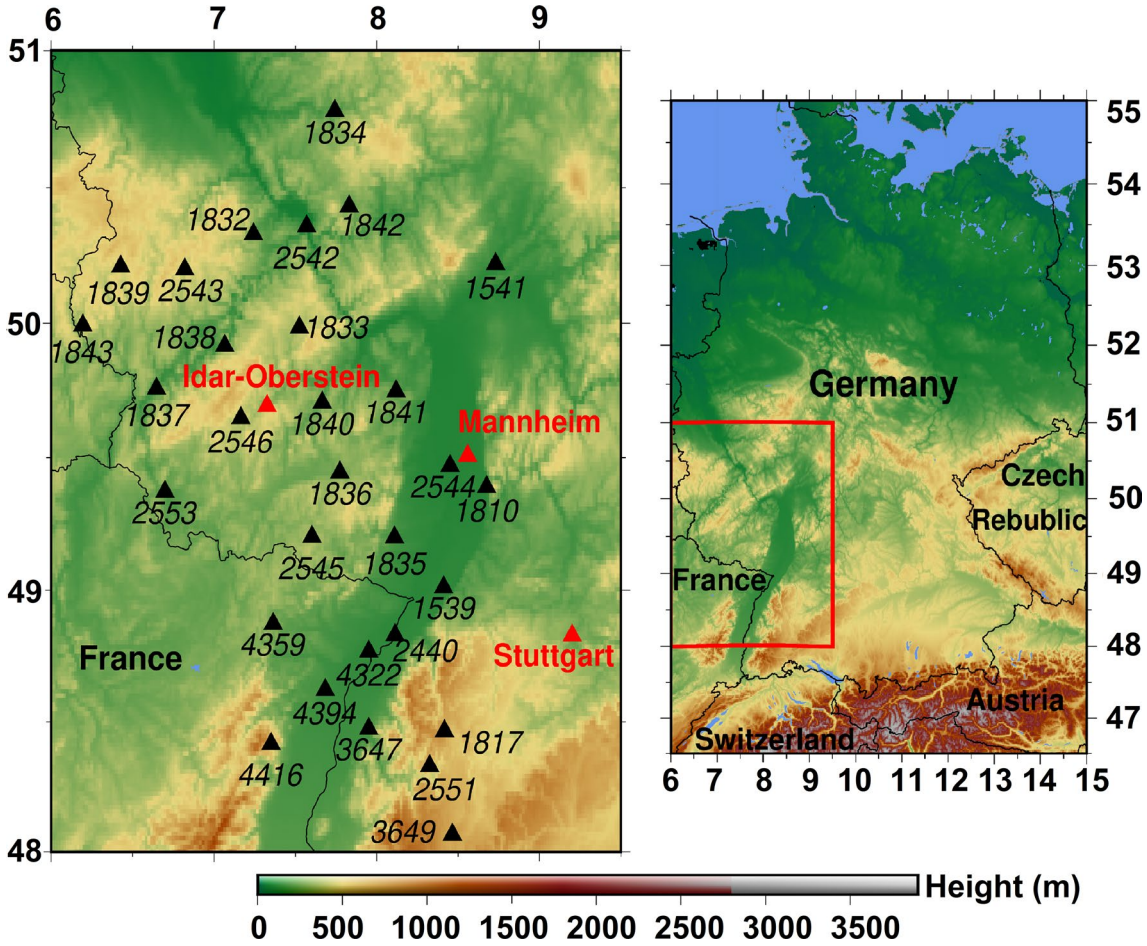

Fig. 2 Topography of the study area together with the location of GNSS and radiosonde stations, black and red triangles, respectively. The numbers aside the black triangles are the names of GNSS stations

each pair of pixels, the most appropriate Copula to model dependence structure is then identified among Gaussian, Clayton, Gumbel, Frank and AMH Copulas (Table 1).

We firstly estimate univariate marginal distributions from the hourly N_w time series for all 12 km pixels and in each pressure layer (i.e., $N = 19 \times 25 = 475$ pixels) to transform data to the rank space (see 6). Then, the empirical Copula CDF and PDF between each pixel and all other pixels are estimated using the transformed data. Finally, three Copula-based dissimilarity measures λ^1, λ^2 and λ^3 for each pair of pixels are computed. To select the most appropriate dissimilarity measure for optimizing voxel sizes at a pressure level, the degree of asymmetry in the dependence structure of pair pixels is evaluated at that level. To do this, Copula parameters are estimated, and the most suitable one is identified by comparing their AIC and BIC measures.

Once an appropriate dissimilarity measure for each pressure level is identified, the horizontal size of voxels is determined for that level. This is done by investigating the percentage frequency of similar pair pixels with different distances.

Figure 3 indicates the percentage frequencies of λ^1, λ^2 and λ^3 for the pairs of pixels with different distances in some of the pressure levels. In these figures, the percentage of pair pixels is plotted against the distance of pixels for the three dissimilarity measures. In these plots, dissimilarity values of equal or less than 0.1 denote pair pixels with maximum similarity and the values larger than 0.4 belong to the pixels with maximum variations. These thresholds have been driven by the analysis of input data.

According to Fig. 3, by moving upward from the earth surface to the top of the troposphere, observed variations of the estimated dissimilarities decrease. In other words, while all range of dissimilarity values from the minimum to maximum is seen in pixel pairs on the earth surface, at the last pressure level, the maximum estimated value for λ^1 and λ^3 is 0.2 and for λ^2 is 0.3. This shows the insignificant variations of N_w on the top part of the troposphere which is expected due to little water vapor in the upper troposphere.

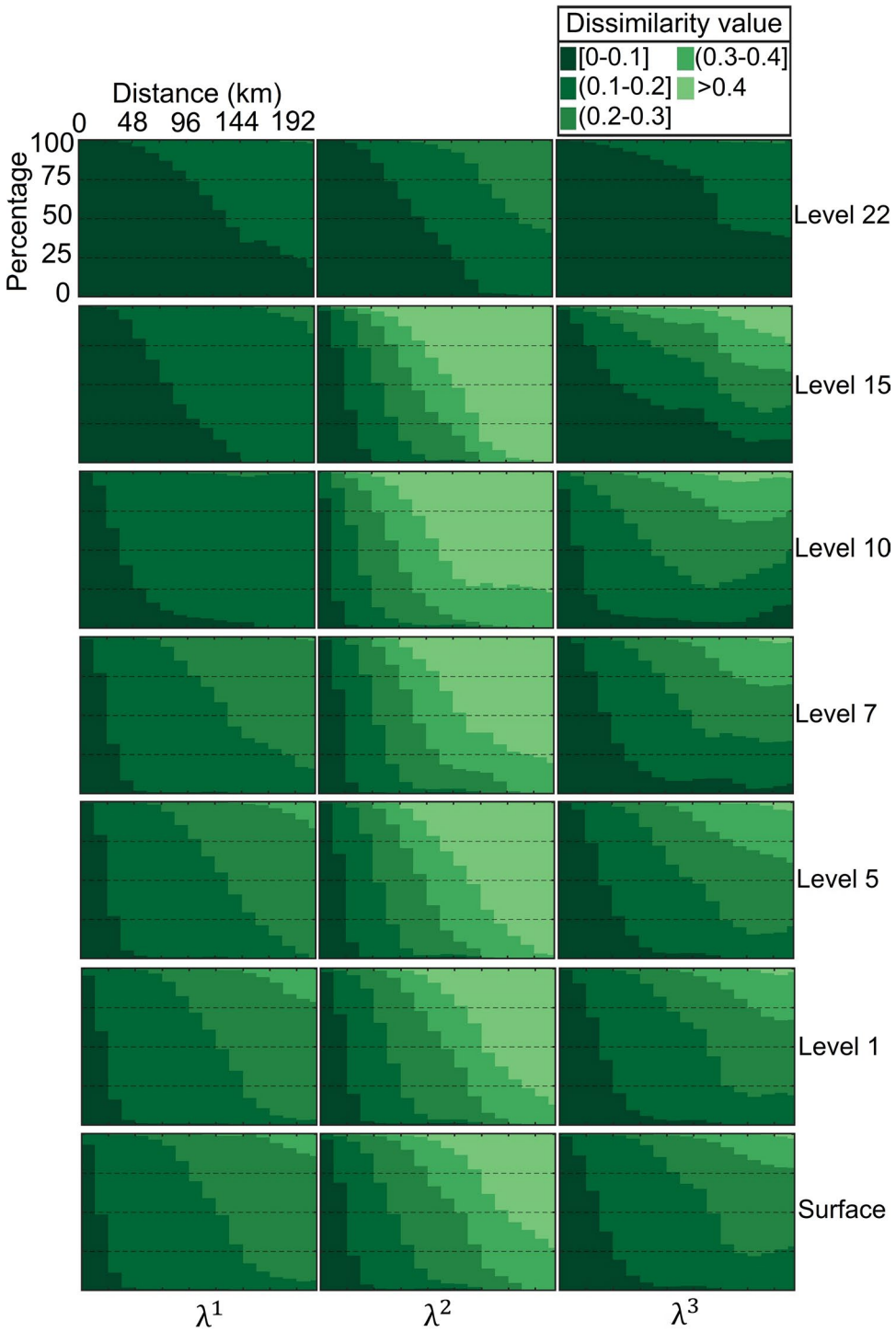

Fig. 3 Investigating the percentage frequency of dissimilarity values λ^1, λ^2 and λ^3 for the pair of pixels with different distances at studied pressure levels. The vertical and horizontal axes are the percentage of pair pixels and the distance of pixels for the dissimilarity measures, respectively

Since wet refractivity depends on meteorological parameters, dissimilarity values between the N_w time series of the evaluated pixels are indications of how similar their atmospheric features are. Therefore, as wet refractivity is our target quantity, its spatial variations can be considered to find an optimal resolution for discretizing our inverse problem.

To this end, if more than 50% of the pixel pairs with a certain distance at a pressure level have maximum similarity reported by the investigated measures (i.e., dissimilarity values ≤ 0.1), we consider the distance as a suitable horizontal model resolution at that level.

Tables 2, 3, 4 list the percentage of the similar pixel pairs with different distances at each pressure level based on λ^1, λ^2 and λ^3 measures. These results and Fig. 3 include the expected variations of meteorological parameters from the ground to the top of the troposphere. According to the

Table 2 Percentage frequency of similar pixels with different distances at different pressure levels based on first dissimilarity measure $(\lambda^1 \leq 0.1)$

Distance of pixels (km)	Earth surface	1	5	7	10	15	22
12	93.7	95.9	99.8	99.1	99.9	100	100
24	48.9	60.3	79.4	77.5	91.5	99.8	100
36	11.6	16.6	27.3	31. − 9	64.3	98.3	99.9
48	2.1	3.4	5.2	8.5	40.5	91.8	99.0
60	1.0	1.3	2.0	2.0	25.7	79.8	96.5
72	0.9	1.0	1.2	1.0	16.4	66.3	92.2
84	0.9	0.9	1.0	0.9	11.7	51.7	87.2
96	0.9	0.9	1.0	1.0	8.5	37.5	80.9
108	0.9	1.0	1.1	1.1	7.1	28.3	74.2
120	1.0	1.1	1.3	1.2	6.4	22.4	65.3
132	0.9	1.1	1.3	1.3	5.2	14.9	55.6
144	0.6	0.6	0.7	0.6	4.1	7.0	44.9
156	0	0	0	0	4.0	0.7	35.0
168	0	0	0	0	0.9	0	37.0
180	0	0	0	0	0.4	0	32.6
192	0	0	0	0	0	0	27.0
204	0	0	0	0	0	0	24. 7
216	0	0	0	0	0	0	18.7

Table 3 Percentage frequency of the pairs of similar pixels with different distances at different pressure levels based on second dissimilarity measure $(\lambda^2 \leq 0.1)$

Distance of pixels (km)	Earth surface	1	5	7	10	15	22
12	96.8	98.2	99.4	98.8	83.5	97.5	100
24	69.3	71.3	67.1	66.7	17.3	73.6	100
36	22.4	20.2	10.5	7.4	2.2	33.8	98.7
48	4.2	2.7	1.2	1.3	1.0	8.9	94.7
60	1.3	1.2	1.1	0.9	0.7	1.3	86.0
72	1.2	1.2	1.0	0.8	0.7	1.1	74.2
84	1.2	1.1	1.0	0.8	0.7	1.1	62.9
96	1.2	1.2	1.0	0.8	0.7	1.1	51.7
108	1.4	1.3	1.1	0.9	0.7	1.2	41.4
120	1.6	1.5	1.3	1.0	0.8	1.4	33.6
132	1.5	1.4	1.2	1.1	0.8	1.4	23.6
144	0.9	0.7	0.7	0.6	0.4	0.7	11.2
156	0	0	0	0	0	0	2.6
168	0	0	0	0	0	0	2.5
180	0	0	0	0	0	0	1.6
192	0	0	0	0	0	0	0.9
204	0	0	0	0	0	0	0.5
216	0	0	0	0	0	0	0.6

results, by approaching to the end of the troposphere, the similarity between pixels, which are far from each other, increases so that. We can see the maximum similarity even between the farthest pixels (i.e., 216 km distance); however, there are no similar pixels more than 144 km apart on the earth surface. Furthermore, at this level, based on λ^1 and λ^2, the percentage of similar pixels with more than 36 km distance is negligible, and according to λ^3, the percentage of similar pixels that are more than 60 km apart is insignificant.

Table 5 illustrates horizontal resolutions proposed by each of the Copula-based dissimilarity measures concluded from Tables 2, 3, 4. According to Table 5, proposed

Table 4 Percentage frequency of the pairs of similar pixels with different distances at different pressure levels based on third dissimilarity measure $(\lambda^3 \leq 0.1)$

Distance of pixels (km)	Earth surface	1	5	7	10	15	22
12	98.8	99.4	99.9	100	89.2	98.1	100
24	86.7	91.0	95.5	96.5	53.0	89.3	99.9
36	63.8	69.3	74.0	78.4	21.8	75.0	99.0
48	37.9	41.9	47.2	52.4	12.0	60.4	97.4
60	19.8	20.3	27.2	32.2	8.8	50.9	95.4
72	9.6	9.7	14.9	21.2	7.6	44.6	93.3
84	5.2	6.0	7.4	14.6	7.1	41.1	90.8
96	2.8	3.7	4.0	10.5	6.8	37.0	87.9
108	2.6	2.9	3.3	8.2	6.5	34.3	84.3
120	3.1	3.4	3.5	8.2	5.2	35.3	82.0
132	2.9	3.4	3.7	9.6	4.4	34.8	77.8
144	1.8	1.8	2.5	10.0	4.4	26.3	66.5
156	0	0.2	0.5	9.9	4.0	20.9	46.8
168	0	0	0	6.7	4.3	16.1	42.8
180	0	0	0	3.4	7.0	13.7	42.0
192	0	0	0	3.5	10.7	14.9	41.9
204	0	0	0	5.0	14.6	15.1	39.5
216	0	0	0	6.8	15.2	15.1	38.4

Table 5 Appropriate horizontal resolution at each pressure level based on Copula-based dissimilarity measures λ1, λ2 and λ3

Pressure level	Horizontal resolution based on λ1 (km)	Horizontal resolution based on λ2 (km)	Horizontal resolution based on λ3 (km)
Earth surface	12	24	36
1	24	24	36
5	24	24	36
7	24	24	36
10	36	12	24
15	84	24	60
22	132	96	144

resolutions differ from one dissimilarity measure to another and changes from the earth surface and upwards. They were expected due to the different characteristics of the dissimilarity measures: λ^1 is an appropriate measure for analyzing data with symmetric dependence structure, while λ^2 and λ^3 can model the asymmetry of the Copulas as well. Since λ^3 is free of individual adapting of observations for Spearman's rank correlation and considers the time-lagged related dependence, it outperforms λ^2. Therefore, the suitable dissimilarity measure for selecting horizontal resolution at each level should be determined by investigating the appropriate Copula for modeling the dependence structure of pixel pairs at that level.

Table 6 indicates the percentage of pixel pairs with the dependence structure of the intended Copulas at different pressure levels. Among all evaluated Copulas in this study, Gaussian and Frank Copulas are symmetric. In contrast, the Gumbel Copula is asymmetric in the upper tail and implies more dependency between large values of time series. Moreover, the asymmetric Clayton and AMH Copulas indicate lower tail dependence which is much stronger in the Clayton.

Table 6 Percentage of the pairs of pixels with the dependence structure of different Copulas at different pressure levels

Pressure level	Gaussian	Frank	Clayton	Gumbel	AMH
Earth surface	68	7	24	1	0
1	69	11	18	2	0
5	77	8	14	1	0
7	77	14	8	1	0
10	54	45.5	0	0.5	0
15	0	29	0	71	0
22	0	74	0	26	0

Table 7 illustrates the percentage of pixel pairs with symmetric and asymmetric dependence structures at each pressure level. According to this table, asymmetry in the dependence structure of estimated N_w values at all pressure levels is significant except for level 10, where 99.5% of pixel pairs are symmetric.

According to the above discussion, to identify the horizontal resolution of the tomography network at each pressure level, we analyze the percentage of pixel pairs with maximum similarity at a certain distance together with the percentage of symmetric and asymmetric Copulas. If more than 95% of the evaluated pixels are symmetric, λ^1 is applied; otherwise, λ^3 is selected as the appropriate dissimilarity measure. Therefore, based on Tables 6 and 7, the appropriate dissimilarity measure for tropospheric modeling at all pressure levels is λ^3 except for level 10, in which λ^1 is the most appropriate one.

Table 7 Percentage of the pairs of pixels with symmetric and asymmetric dependence structure at different pressure levels

Pressure level	Symmetric Copulas	Asymmetric Copulas
Earth surface	75	25
1	80	20
5	85	15
7	91	9
10	99.5	0.5
15	29	71
22	74	26

Table 8 indicates the average of the estimated dissimilarity values for pixel pairs with different distances at each pressure level. According to this table, by increasing the distance of pixels, the mean values of the dissimilarity measures increase. The minimum mean values (dissimilarity values ≤ 0.1) with maximum distance between pixels, i.e., 144 km are seen at the last pressure level.

As a result, our Copula-based method suggests non-uniform sizes for the voxels in the tomography network of the study area. More specifically, the proposed voxel sizes for the tomography model are 36 km from the earth surface to level 10, 60 km at level 15 and 144 km at level 22.

The GPS networks are developed for positioning and navigation. Therefore, the satellite–receiver relative configurations are not optimal for GPS tomography. Moreover, atmospheric parameters are not constant. This renders non-uniqueness of the solution. The contribution of the imaging geometry to the inverse solution is usually evaluated using the resolution matrix of the model. Using the approximate position of the GPS stations (refer to Fig. 2) and the satellite ephemerides for the DoY 279, in 2016 and assuming a time resolution of 1 h, we computed resolution matrices for several models with different voxel sizes. Similar to our Copula-based assessments, investigated voxel sizes are multiples of 12 km, i.e., 12, 24, 36, 48, 60, etc. The Computed resolutions show how the quality of inverse solution changes with the size of voxels. According to these results, the resolution matrix is the identity matrix

Table 8 Mean values of the appropriate dissimilarity measure for each pressure level of pixel pairs with different distance

Distance of pixels (km)	Earth surface	1	5	7	10	15	22
12	0.05	0.04	0.04	0.03	0.06	0.03	0.02
24	0.07	0.07	0.06	0.06	0.08	0.06	0.03
36	0.09	0.09	0.09	0.08	0.09	0.07	0.04
48	0.11	0.10	0.10	0.10	0.10	0.10	0.05
60	0.12	0.12	0.12	0.11	0.11	0.11	0.05
72	0.13	0.13	0.14	0.13	0.12	0.12	0.05
84	0.15	0.14	0.15	0.15	0.13	0.14	0.06
96	0.16	0.16	0.17	0.16	0.13	0.14	0.06
108	0.17	0.17	0.18	0.18	0.14	0.15	0.06
120	0.18	0.18	0.20	0.19	0.14	0.16	0.06
132	0.19	0.19	0.21	0.20	0.15	0.16	0.07
144	0.20	0.21	0.23	0.22	0.14	0.19	0.08
156	0.22	0.23	0.24	0.22	0.14	0.22	0.10
168	0.23	0.24	0.25	0.23	0.14	0.24	0.11
180	0.24	0.25	0.26	0.24	0.14	0.25	0.11
192	0.24	0.26	0.27	0.24	0.14	0.26	0.11
204	0.25	0.26	0.27	0.24	0.14	0.26	0.11
216	0.24	0.26	0.27	0.24	0.14	0.26	0.11

when the horizontal resolution of the model decreases to 108 km. Since water vapor is highly variable (in particular near the earth surface), applying a model with this element size is not meaningful. On the other hand, the proposed method is geometry-free or it proposes voxel sizes without any information on the imaging geometry, especially the distribution of GPS stations in the test area. Indeed, it suggests the optimum voxel sizes based on the information

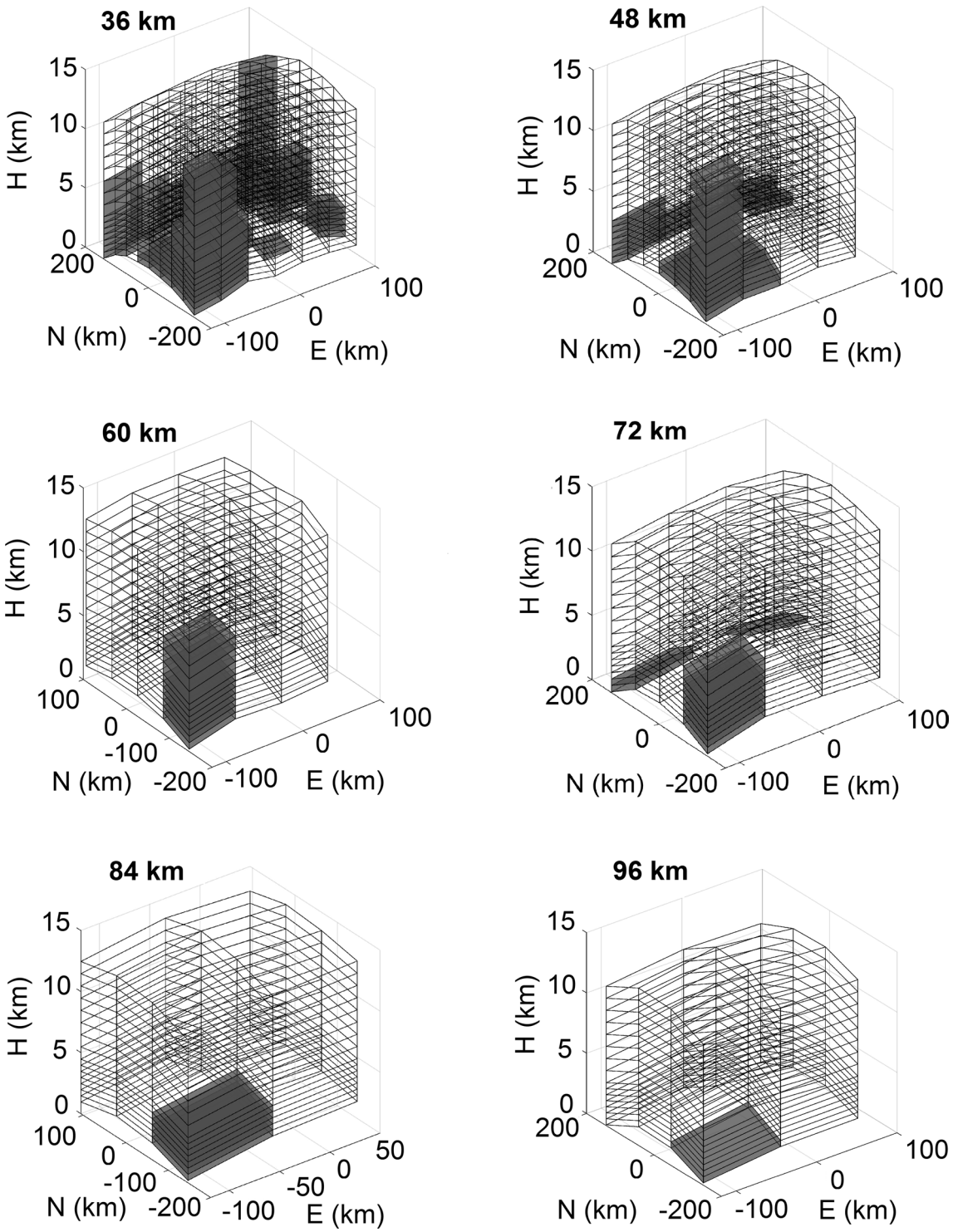

Fig. 4 Tomography models with different resolutions (36, 48, 60, 72, 84 and 96 km) for first epoch of DoY 279. Empty voxels are indicated by gray

available on the atmospheric dynamics. Once the method is applied for a certain period of time, we have a strong measure for the dynamics besides the geometric information derived from the analysis of resolution matrices to propose an optimum resolution for a tomography model.

To clarify this, we illustrate the model parameters that are smeared out (when only the spatial variations are concerned) in Fig. 4. Such parameters are given in gray. As expected, empty voxels mostly belong to the resolution of 36 km and there are no empty elements in the voxel size of 108 km.

The dynamics and geometry in GPS tomography show that using such uniform voxel sizes for a model results in missing information in the lower parts of the troposphere and redundancy on its top. That is, to keep the dynamics of the problem intact; the application of voxels with different sizes is inevitable.

Applying the Copula-based approach as an absolute dynamic technique has the following significant results: To preserve the spatial variation of water vapor, using a model with hybrid voxel sizes is inevitable. Moreover, a dense GPS network like the one in Germany is neither sufficient for tomographic reconstruction of humidity nor for reconstructing its variations in space and time. This is seen through the top views of our tomography network given in the right-hand side plots in Fig. 5.

According to Fig. 3, the resolution of 48 km preserves the horizontal variations of the wet refractivity intact in 37.9%, 41.9%, 47.2%, 52.4% and 40.5% of the model parameters at the earth surface and levels 1, 5, 7 and 10, respectively (see Table 4 for levels 1–10 and Table 2 for level 10). Moreover, based on Fig. 5, reducing the model resolution from 36 to 48 km at these pressure layers can significantly reduce the number of model parameters that are smeared out in this part. This decreases the number of empty voxels from 37.5% of elements in 36–25% in 48 km. This comparison provides a compromise between the resolution of reconstructed images and spatial variations of the sought parameter in this experiment. Moreover, according to Fig. 4, by reducing the spatial resolution of the tomography model to 96 km, it is not still possible to reconstruct the wet refractivity with a reasonable resolution in the area of $48.31 \leq \varphi \leq 48.85$ and $5.98 \leq \lambda \leq 6.70$. This area is located in France, and the insufficiency of available GNSS stations in the area is shown in Fig. 2.

Summary and conclusion

In this paper, a geometry-free method for optimal tomographic reconstruction of water vapor has been proposed. We apply a Copula-based approach for investigating dependence structure and dissimilarity of wet refractivities (N_w). Meteorological parameters required for estimating N_w in each voxel are calculated from a high-resolution WRF model. The evaluation is performed in southwest Germany and part of France from April to October 2016 at seven pressure levels, so that, for all pixel pairs at a level, i.e., each pixel and all other pixels across the study area, the appropriate Copula for dependence modeling and Copula-based dissimilarity measures are estimated. Furthermore, we evaluate the consistency of results with the imaging geometry by investigating the resolution matrix of our model in all epochs of DoY 279 as a sample.

Since N_w as an unknown parameter in tomography is a function of pressure, temperature and humidity, dissimilarity values between the N_w time series of neighbor pixels indicate how the characteristics of the atmosphere change. Therefore, the optimum horizontal resolution at each level is determined by investigating the distance-based variation of the estimated dissimilarities. As a preliminary step, the most appropriate dissimilarity measure at each level is identified by analyzing the dependence structure of all evaluated pixel pairs. If the dependence structure of more than 95% of investigated pixels is symmetric, λ^1 is applied; otherwise, λ^3 has been selected as the preferred measure. According to the obtained results, at all pressure levels except level 10 our decision is based on λ^3.

In conclusion, we propose a tomography network whose horizontal resolution changes from the earth surface to the top of the troposphere for the evaluated time period in our study area. More precisely, to keep the dynamics of the wet refractivities intact, the optimal design will be realized using three different voxel sizes: 36 km from the earth surface to level 10 (mean height of 2.2 km), 60 km in level 15 (mean height of 4.8 km) and 144 km in level 22 (mean height of 10 km). By increasing the distance of pixels, the mean values of the dissimilarity measures increase. Thus, minimum mean values (dissimilarity values ≤ 0.1) for pixel pairs in the maximum distance (144 km) are seen on top of the troposphere. Furthermore, investigating the resolution matrix of the model in DoY 279 reveals that a uniform tomography network with a horizontal resolution of 108 km guarantees a unique solution. However, water vapor is highly variable, in particular near to the earth surface, and therefore, using such dimension falsifies the assumption of the homogeneity in the model elements. That is, using uniform voxel sizes results in false information in the lower parts of the troposphere.

According to our results, the current density of GPS stations in the study area is not sufficient for tomographic reconstructions of the wet refractivity that preserves the spatial variations of N_w and guarantees the uniqueness of the solution.

Our proposed method is geometry-free because it is independent of any information on the distribution of

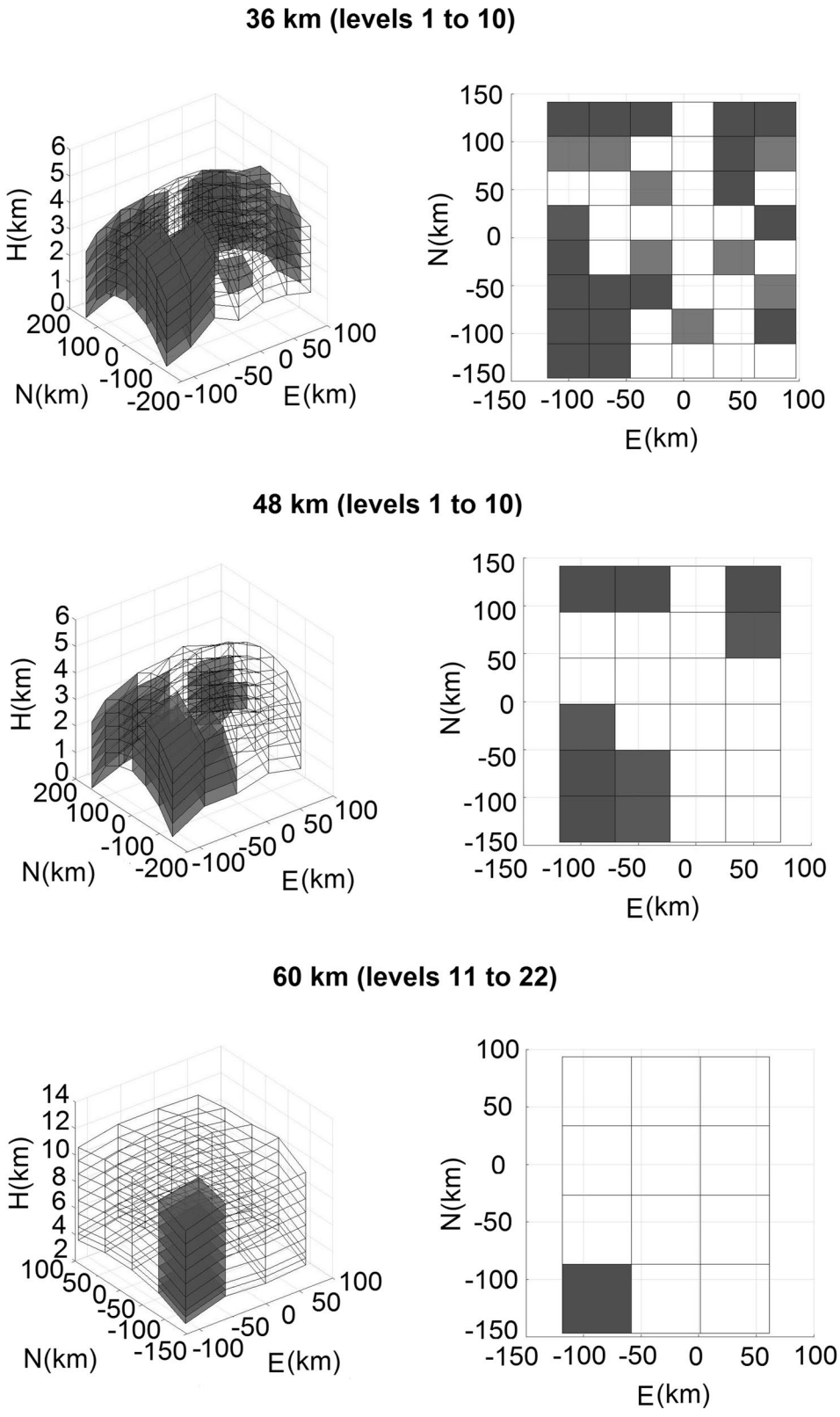

Fig. 5 Side and top views of tomography model reconstructed by the Copula-based proposed resolutions for first epoch of DOY 279. Empty voxels are indicated by gray

GNSS stations. Moreover, it suggests voxel sizes in terms of atmospheric dynamics for a long period of time, the period of April to October 2016 in this study. Therefore, once the method is applied in a certain period of time, we have a dynamic measure besides the geometric one to propose an optimized tomography model in the validity time

of the corresponding copula-based results. As we showed, combining our Copula-based method and resolution matrix provides a mathematical tool for deciding on the required compromise between the geometry and dynamics in GPS tomography.

It has to be emphasized that since the WRF model is limited to 6 months, the proposed tomographic model may miss some seasonal features if strong seasonal variations exist. Furthermore, the noise of measurements is a challenge when the redundancy is low: in real-time or near-real-time application where the permitted latency is only a couple of minutes or even less, if possible. Here, the redundancy is at least 3000 therefore the effect of noise is negligible.

Acknowledgements This study was funded by scholarships from K. N. Toosi University of Technology and the Karlsruhe Institute of Technology—Institute of Meteorology and Climate Research, Atmospheric Environmental Research. It was enabled additionally by funds from the German Research Foundation (DFG-ATMOWATER, KU 2090/10) and the German Ministry of Science and Education (BMBF)-funded GROW-SaWaM project. We would further like to thank the German Research Center for Geosciences (GFZ) for providing the GNSS data.

Data availability The GNSS station positions were provided by the GFZ upon our request. For meteorological data and the WRF-Hydro model refer to http://doi.org/10.5281/zenodo.3405780 in Fersch et al. 2020. Moreover, the satellite ephemerides are available from http://navigation-office.esa.int/GNSS_based_products.html

References

Adavi Z, Mashhadi-Hossainali M (2014) 4D tomographic reconstruction of the tropospheric wet refractivity using the concept of virtual reference station, case study: northwest of Iran. Meteorol Atmos Phys 126:193–205. https://doi.org/10.1007/s00703-014-0342-4

Ang A, Chen J (2002) Asymmetric correlations of equity portfolios. J Financ Econ 63:443–494. https://doi.org/10.1016/S0304-405X(02)00068-5

Arbenz P (2013) Bayesian copula distributions, with application to operational risk management—some comments. Methodol Comput Appl Probab 15:105–108. https://doi.org/10.1007/s11009-011-9224-0

Aster RC, Borchers B, Thurber CH (2018) Parameter estimation and inverse problems. Elsevier

Bardossy A (2006) Copula based geostatistical models for groundwater quality parameters. Water Resour Res. https://doi.org/10.1029/2005WR004754

Bevis M, Businger S, Herring TA, Rocken C, Anthes RA, Ware RH (1992) GPS meteorology: remote sensing of atmospheric water vapor using the global positioning system. J Geophys Res: Atmos 97:15787–15801. https://doi.org/10.1029/92JD01517

Bevis M, Businger S, Chiswell S, Herring TA, Anthes RA, Rocken C, Ware RH (1994) GPS meteorology: mapping zenith wet delays onto precipitable water. J Appl Meteorol 33:379–386

Bi Y, Mao J, Li C (2006) Preliminary results of 4-d water vapor tomography in the troposphere using GPS. Adv Atmos Sci 23:551–560. https://doi.org/10.1007/s00376-006-0551-y

Charpentier A, Fermanian JD, Scaillet O (2007) The estimation of copulas: theory and practice. Copulas: from Theory Appl in Financ 89:35–64

Chen B, Liu Z (2014) Voxel-optimized regional water vapor tomography and comparison with radiosonde and numerical weather model. J Geodesy 88:691–703. https://doi.org/10.1007/s00190-014-0715-y

Cherubini U, Luciano E, Vecchiato W (2004) Copula methods in Finance. Wiley

de Haan S, Holleman I, Holtslag AA (2009) Real-time water vapor maps from a GPS surface network: construction, validation, and applications. J Appl Meteorol Climatol 48:1302–1316. https://doi.org/10.1175/2008JAMC2024.1

Dee DP et al (2011) The Era-Interim reanalysis: Configuration and performance of the data assimilation system. Q J R Meteorol Soc 137:553–597. https://doi.org/10.1002/qj.828

Deheuvels P (1979) La fonction de d´ependance empirique et ses propri´et´es. un test non param´etrique d'ind´ependance. Bulletins de l'Acad´emie Royale de Belgique 65, 274–292.

Embrechts P, Lindskog F, McNeil A, (2001) Modelling dependence with copulas. Rapport technique, D´epartement de math´ematiques, Institut Federal de Technologie de Zurich, Zurich 14:1-50

Fang Y, Madsen L, Liu L (2014) Comparison of two methods to check copula fitting. Int J Appl Math 44:354

Fersch B, Senatore A, Adler B, Arnault J, Mauder M, Schneider K, Volksch I, Kunstmann H (2020) High-resolution fully coupled atmospheric–hydrological modeling: a cross-compartment regional water and energy cycle evaluation. Hydrol Earth Syst Sci 24:2457–2481. https://doi.org/10.5194/hess-24-2457-2020

Gendt G, Dick G, Reigber C, Tomassini M, Liu Y, Ramatschi M (2004) Near real time GPS water vapor monitoring for numerical weather prediction in Germany. J Meteorol Soc Japan. Ser II 82:361–370. https://doi.org/10.2151/jmsj.2004.361

Goshtasby AA (2012) Similarity and dissimilarity measures. Image registration. Springer, Cham, pp 7–66

Guloksuz CT (2016) Comparison of some selection criteria for selecting bivariate archimedean copulas. A K U Fen Muhendis Bilimleridergisi 16:250–255

Huard D, Evin G, Favre AC (2006) Bayesian Copula selection. Comput Stat Data Anal 51:809–822. https://doi.org/10.1016/j.csda.2005.08.010

Joe H (1997) Multivariate models and multivariate dependence concepts. CRC Press

Lee SW, Kouba J, Schutz B, Kim DH, Lee YJ (2013) Monitoring precipitable water vapor in real-time using global navigation satellite systems. J Geodesy 87:923–934. https://doi.org/10.1007/s00190-013-0655-y

Lorenz C, Montzka C, Jagdhuber T, Laux P, Kunstmann H (2018) Long-term and high-resolution global time series of brightness temperature from copula-based fusion of SMAP enhanced and SMOS data. Remote Sens 10:1842. https://doi.org/10.3390/rs10111842

Menke W (1989) Geophysical data analysis: discrete inverse theory. International Geophysics Series

Mikosch T (2006) Copulas: tales and facts. Extremes 9:3–20. https://doi.org/10.1007/s10687-006-0015-x

Modiri S, Belda S, Heinkelmann R, Hoseini M, Ferrandiz JM, Schuh H (2018) Polar motion prediction using the combination of SSA and Copula-based analysis. Earth, Planets Space 70:1–18. https://doi.org/10.1186/s40623-018-0888-3

Modiri S, Belda S, Hoseini M, Heinkelmann R, Ferrandiz JM, Schuh H (2020) A new hybrid method to improve the ultra-short-term prediction of LOD. J Geodesy 94:23. https://doi.org/10.1007/s00190-020-01354-y

Mousavian R, Lorenz C, Hossainali MM, Fersch B, Kunstmann H (2021) Copula-based modeling of dependence structure in geodesy and GNSS applications: case study for zenith tropospheric delay in complex terrain. GPS Solut 25:1–17. https://doi.org/10.1007/s10291-020-01044-4

Nelsen RB (2006) An introduction to Copulas. Springer series in statistics, 2nd edn. Springer, Berlin

Notarpietro R, Cucca M, Gabella M, Venuti G, Perona G (2011) Tomographic reconstruction of wet and total refractivity fields from GNSS receiver networks. Adv Space Res 47:898–912. https://doi.org/10.1016/j.asr.2010.12.025

Rohm W (2012) The precision of humidity in GNSS tomography. Atmos Res 107:69–75. https://doi.org/10.1016/j.atmosres.2011.12.008

Rohm W, Bosy J (2009) Local tomography troposphere model over mountains area. Atmos Res 93:777–783. https://doi.org/10.1016/j.atmosres.2009.03.013

Sadeghi E, Mashhadi Hossainali M, Safari A (2022) Development of a hybrid tomography model based on principal component analysis of the atmospheric dynamics and GPS tracking data. GPS Solut 26(3):1–13. https://doi.org/10.1007/s10291-022-01264-w

Samaniego L, Bardossy A, Kumar R (2010) Streamflow prediction in ungauged catchments using Copula-based dissimilarity measures. Water Resour Res. https://doi.org/10.1029/2008WR007695

Skamarock WC, Klemp JB, Dudhia J, Gill DO, Barker D, Duda MG, Powers JG (2008) A description of the advanced research WRF version 3. NCAR technical note NCAR/TN-475+STR. National Center for Atmospheric Research, Boulder. https://doi.org/10.5065/D68S4MVH

Sklar A (1959) Fonctions de repartition a n dimensions et leurs marges. Publ Inst Statist Univ Paris 8:229–231

Vaquero-Martınez J, Anton M (2021) Review on the role of GNSS meteorology in monitoring water vapor for atmospheric physics. Remote Sens 13:2287. https://doi.org/10.3390/rs13122287

Vogl S, Laux P, Qiu W, Mao G, Kunstmann H (2012) Copula-based assimilation of radar and gauge information to derive bias-corrected precipitation fields. Hydrol Earth Syst Sci 16:2311–2328. https://doi.org/10.5194/hess-16-2311-2012

Yao Y, Zhao Q (2017) A novel, optimized approach of voxel division for water vapor tomography. Meteorol Atmos Phys 129:57–70. https://doi.org/10.1007/s00703-016-0450-4

Roya Mousavian received her MSc and Ph.D. degrees in Geodesy from K. N. Toosi University of Technology in 2013 and 2021, respectively. She completed a research visit at the Institute of Meteorology and Climate Research (IMK-IFU) of Karlsruhe Institute of Technology (KIT) in 2018 and 2019. Her research interests are GNSS meteorology, satellite geodesy and slow earthquakes.

Masoud Mashhadi Hossainali is an associate professor in Geodesy at K. N. Toosi University of Technology. He received his Ph.D. degree at the Darmstadt University of Technology. His current research interests are GNSS meteorology, deformation monitoring and constellation design for various space mission.

Christof Lorenz is a postdoctoral researcher at the Campus Alpin of the Karlsruhe Institute of Technology. He studied Geodesy and Geoinformatics at the University of Stuttgart and did his Ph.D. in climate and environmental sciences at the University of Augsburg. His current research focuses on the development of empirical–statistical data fusion approaches, especially for seasonal hydrometeorological predictions and remote sensing information.

Harald Kunstmann is a professor and chair for regional climate and hydrology at the University of Augsburg in a joint appointment with Karlsruhe Institute of Technology (Campus Alpin). His current research focuses on observation and modeling of the coupled atmospheric–terrestrial water cycle for different regions worldwide.